The Cell Surface 9 (2023) 100092

Contents lists available at ScienceDirect

The Cell Surface

journal homepage: www.sciencedirect.com/journal/the-cell-surface

Characterizing the role of phosphatidylglycerol-phosphate phosphatases in *Acinetobacter baumannii* cell envelope biogenesis and antibiotic resistance

Maoge Zang [a], Alice Ascari [a,b], Felise G. Adams [a], Saleh Alquethamy [a], Bart A. Eijkelkamp [a,*]

[a] Molecular Sciences and Technology, College of Science and Engineering, Flinders University, Adelaide, South Australia 5042, Australia
[b] Department of Molecular and Biomedical Science, School of Biological Sciences, University of Adelaide, Adelaide 5005, Australia

ARTICLE INFO

Keywords:
Cell envelope
Phospholipids
Desaturase
Peptidoglycan
Antibiotic resistance

ABSTRACT

The dissemination of multi-drug resistant *Acinetobacter baumannii* threatens global healthcare systems and necessitates the development of novel therapeutic options. The Gram-negative bacterial cell envelope provides a first defensive barrier against antimicrobial assault. Essential components of this multi-layered complex are the phospholipid-rich membranes. Phosphatidylglycerol phosphate (PGP) phosphatases are responsible for a key step in the biosynthesis of a major phospholipid species, phosphatidylglycerol (PG), but these enzymes have also been implicated in the biogenesis of other cell envelope components. Our bioinformatics analyses identified two putative PGP candidates in the *A. baumannii* genome, PgpA and PgpB. Phospholipid analyses of isogenic *pgpA* mutants in two distinct *A. baumannii* strains revealed a shift in the desaturation levels of phosphatidylethanolamine (PE) phospholipid species, possibly due to the activation of the phospholipid desaturase DesA. We also investigated the impact of the inner membrane phosphatases on other cell envelope components, which revealed a role of PgpB in the maintenance of the *A. baumannii* peptidoglycan layer, and consequently carbapenem resistance. Collectively, this work provides novel insights into the roles of PGP phosphatases on the global lipidomic landscape of *A. baumannii* and their interconnectivity with the biogenesis of other cell envelope components. The non-essentiality of these candidates exemplifies metabolic versatility of *A. baumannii*, which is believed to be key to its success as global pathogen.

Introduction

The Gram-negative, opportunistic bacterial pathogen *Acinetobacter baumannii* thrives in the hospital environment, where pan drug-resistant infections are associated with increased mortality rates (Karakonstantis et al., 2020). The escalating development of multi-drug resistant (MDR) isolates across the world stems from successful dissemination and a formidable ability to rapidly adapt during antibiotic pressure (Hamidian and Nigro, 2019, Harding et al., 2017). Although various drug-specific resistance mechanisms have been studied, the primary mode of antibiotic defense is the *A. baumannii* envelope with its distinct inner and outer lipid membranes separated by a peptidoglycan layer in the periplasmic space (May and Grabowicz, 2018). While the outer membrane represents an asymmetric assembly with lipopolysaccharide/lipooligosaccharide (LPS/LOS) populating the outer leaflet and phospholipids at the inner leaflet, the inner membrane is primarily composed of phospholipids. Like all bacterial species, *A. baumannii* maintains the integrity of this protective barrier with highly coordinated lipid homeostasis pathways to yield an abundance of diverse phospholipids, including the major species phosphatidylethanolamine (PE), phosphatidylglycerol (PG) and cardiolipin (CL) (Sohlenkamp and Geiger, 2016). Of these, PG and CL are the predominant anionic species synthesized via the same biological pathway, with CL derived from two PG molecules (Parsons and Rock, 2013). These major anionic phospholipids are not only important in maintaining membrane integrity, but also form domains that facilitate protein translocation via the *sec*-dependent pathway and play a key role in determining the site of cell division (Koch et al., 2019, Barák et al., 2008). Further, *A. baumannii* phospholipid domain formation is a known determinant of antibiotic penetration (MacDermott-Opeskin et al., 2022).

The final step of PG synthesis involves the dephosphorylation of the precursor molecule, phosphatidylglycerol phosphate (PGP), which is catalyzed by PGP-phosphatases. To date, three members encoding structurally distinct PGP-phosphatases localized within the inner membrane have been characterized, which includes PgpA, PgpB and PgpC as seen in *Escherichia coli* (Icho and Raetz, 1983, Lu et al., 2011).

* Corresponding author.
E-mail address: bart.eijkelkamp@flinders.edu.au (B.A. Eijkelkamp).

https://doi.org/10.1016/j.tcsw.2022.100092
Received 3 July 2022; Received in revised form 6 December 2022; Accepted 7 December 2022
Available online 10 December 2022

Whereas PgpA and PgpC have been proposed to have cytoplasmic-facing active sites, structural analyses have demonstrated a periplasmic orientation for PgpB, resulting in reduced PGP-phosphatase efficiency (Lu et al., 2011, Tong et al., 2016). This suggests that PgpA and PgpC act as the predominant phosphatases involved in PG biosynthesis in *E. coli*. Interestingly, PgpC is not consistently identified across different bacterial species, as *Helicobacter pylori* was found to lack this particular membrane embedded phosphatase (Gasiorowski et al., 2019). Further, while both PgpA and PgpC have not been implicated to participate in other metabolic pathways, PgpB is defined as a Type 2 phosphatidic acid phosphatase (PAP2). In addition to PgpB, *E. coli* encodes additional PAP2 members, such as LpxT (formerly YeiU) and YbjG, with roles in peptidoglycan biosynthesis (Touzé et al., 2008, Ghachi et al., 2005). This critical process requires the lipid carrier, undecaprenyl phosphate (C55-P), which binds and translocates the peptidoglycan-building polymer GlcNAc-MurNAc-pentapeptide towards the periplasm where penicillin binding proteins (PBPs) catalyze the polymerization and crosslinking of peptidoglycan (Egan et al., 2020). The phosphatase activity of PAP2 proteins and UppP (formerly BacA) (Ghachi et al., 2005) mediate the dephosphorylation of undecaprenyl pyrophosphate (C55-PP) to generate C55-P, which occurs within the cytoplasm and also the periplasm after the removal of its cargo. As such, the periplasmic orientation of PAP2 proteins such as PgpB suggests an involvement in C55-P recycling (Tian et al., 2020).

The proposed dual functionality of PgpB provides insights into the interconnectivity of various biological pathways responsible for cell envelope biogenesis. Indeed, LpxE (PAP2) from *Aquifex aeolicus* has been characterized to also harbor lipid A 1-phosphatase activity, and was reported to participate in peptidoglycan as well as O-antigen biosynthesis (Zhao et al., 2019). Importantly, the PGP-phosphatases, in particular PgpA and PgpB, have been extensively characterized from a biochemical perspective (Lu et al., 2011, Tong et al., 2016, Tian et al., 2020), yet their biological multifunctionality in a cellular context remains relatively elusive. In addition, little is known about PgpA and PgpB candidates in *A. baumannii*, beyond their implicated function in resistance to tobramycin and colistin (Gallagher et al., 2017, Zhu et al., 2020). As such, the present study aims to define the roles of PgpA and PgpB in *A. baumannii* cell envelope biology.

Materials and methods

Bacterial strains and culturing conditions

The two *A. baumannii* isolates used in this study (Table S1), AB5075_UW and ATCC 17978, were routinely cultured overnight at 37℃ in Lysogeny Broth (LB) with shaking or LB agar (1.5 %). The transposon mutants of AB5075_UW, *pgpA*::T26 and *pgpB*::T26, were purchased from the Manoil laboratory (University of Washington). The *A. baumannii* ATCC 17978 Δ*pgpA*, Δ*pgpA*Δ*desA* and Δ*pgpB* mutants were generated using an established strategy (Adams et al., 2018), with the oligonucleotides listed in Table S2.

Complementation of the A. baumannii pgpA::T26 mutant

Complementation of the *pgpA*::T26 mutant was performed by amplifying *pgpA* with ~ 1 kb up- and downstream flanking regions from AB5075_UW (Table S2). Complementation was achieved through an established strategy (Tickner et al., 2021), using natural transformation of the primary PCR product into the transposon mutant. Briefly, overnight cultures of *pgpA*::T26 were diluted to OD_{600} of 0.05 in fresh LB media (20 ml) and grown to $OD_{600} = 1$. Cells were then further diluted in Tryptone Medium (5 $g.L^{-1}$), and equal volumes of cells and DNA (200 ng.mLng.mL^{-1}) were mixed together, of which 2.5 µl of the suspension was spotted onto Tryptone Medium containing 2 % low electro-endosmosis agarose (Sigma Aldrich) in a microfuge tube. Following overnight incubation at 37 °C, cells were resuspended in 300 µl of LB media and plated onto LB agar containing 250 $µg.mL^{-1}$ gentamicin to identify successful transformants, which were PCR confirmed.

Antimicrobial resistance analyses

The antibiotic susceptibility profiles of *A. baumannii* were determined using the micro-dilution method with cation-adjusted Mueller Hinton media, as described previously (Wiegand et al., 2008). Plates were sealed with a breathable film, placed in a humidity box and incubated overnight at 37 °C. Following incubation, final cell growth (OD_{600}) was determined in a SPECTROstar NANO Spectrophotometer (BMG Labtech), and normalized against the growth of cells without antibiotic supplementation, using GraphPad Prism 9.0.

Bioinformatics

Structural predictions of *A. baumannii* PgpA (ABUW_0091) and PgpB (ABUW_0845) from AB5075_UW were performed using ColabFold, which utilizes AlphaFold 2.0 for structural analyses (Mirdita et al., 2022). Five models were generated from each prediction, in which model 1, representing the prediction of the highest confidence, is used for structural analysis in this study. All structural illustrations were prepared using the molecular visualization program ChimeraX v1.4 (Pettersen et al., 2021), in which *A. baumannii* PgpA and PgpB structures were superimposed onto homologous protein structures of *E. coli* PgpA (AF-P18200-F1) from the AlphaFold 2.0 database and PgpB (PDB: 5JWY) (Tong et al., 2016).

A global diversity network of 292 complete *A. baumannii* genomic assemblies were derived from the PATRIC Bioinformatics Resource Center (Davis et al., 2020). The sequence conservation and prevalence of AB5075_UW (GenBank accession number: CP008706.1) gene products *pgpA*::T26 (ABUW_0091) and *pgpB*::T26 (ABUW_0845) were compared across 292 genomic assemblies using screen assembly v1.2.7 as described previously (Davies et al., 2019, Alquethamy et al., 2022). The parameters used in a BLASTn V2.9.0 search were set to identify targets with 80 % sequence coverage and 80 % sequence identity and above. Hits generated from this search were then translated into corresponding amino acid sequences. Conservation percentages of analyzed genes were determined from a MUSCLE alignment (Edgar, 2004) using Geneious Prime (Kearse et al., 2012). Sites of amino acid variation were determined on homology structural models for both AB5075_UW PgpA and PgpB using ChimeraX v1.4 (Pettersen et al., 2021).

Microscopy

Overnight cultures of *A. baumannii* AB5075_UW wild-type, *pgpA*::T26 and *pgpB*::T26 were diluted to an OD_{600} of 0.05 in fresh LB media (20 mL) and grown to mid-log phase ($OD_{600} = 0.7$). Following washing in phosphate buffered saline (PBS), cells were immobilized on microscope slide glass with poly-L-lysine and visualized at 1000 × magnification using an Olympus BX53 microscope with a UPLXAPO 100 × oil immersion objective. Images were captured with an Olympus DP74 color camera and normalized by white balancing in the Olympus cellSens Dimensions software. Final images were saved as PNG files.

Bacterial lipid extraction

Extraction of *A. baumannii* lipids was performed using a previously established method (Adams et al., 2021a). Overnight cultures of *A. baumannii* AB5075_UW and ATCC 17,978 strains were diluted to an OD_{600} of 0.05 in fresh LB media (20 ml) and grown to mid-log phase ($OD_{600} = 0.7$). Cells were harvested by centrifugation at 7,000 × *g* for 10 min and washed once with PBS, processed pellets were then resuspended in 50 µL of 1.5 % NaCl buffer. For lipid extraction, 1 ml of chloroform:methanol (2:1; v/v) was added to the cell suspension, mixed vigorously for 2 min then incubated at RT for 10 min. Following the

addition of 200 μL 1.5 % NaCl, the cell suspension was mixed vigorously for 1 min and centrifuged at 6,000 × *g* for phase-separation. The lower phase was recovered and concentrated via nitrogen evaporation. All samples were stored at −20℃ prior to gas chromatography/mass spectrometry (GC/MS) analysis.

Phospholipid and fatty acid characterization

The lipidomic profile of phosphatidylglycerol (PG) and phosphatidylethanolamine (PE) in *A. baumannii* lipid extracts, including the number of carbons and double bonds in acyl chains, was determined using Liquid Chromatography-Mass Spectrometry (LC-MS; SAHMRI, Australia) (Adams et al., 2021b).

Lipidomic analyses were performed using a LC-MS system comprising of an Acquity I-class UPLC system (Waters Corporation, Milford, MA, USA) fitted with 100 mm (2.1 mm inner diameter) HSS T3 analytical column (Waters Corporation, Milford, MA, USA) coupled to a Xevo G2-XS Q-Tof mass spectrometer (Waters Corporation, Wilmslow, UK). Lyophilized samples were reconstituted in 90 μl of 1:1 v/v acetonitrile:propan-2-ol, of which 5 μl was injected for both positive and negative ion mode acquisitions. Mobile phase A was made up by combining 800 ml of water with 1.26 g of ammonium formate and 1200 ml of acetonitrile. Mobile phase B was a mixture of 200 ml acetonitrile and 1800 ml propan-2-ol, after which 1.26 g of ammonium formate (dissolved in 2 ml water) was added. The flowrate was set at 0.4 mL. min^{-1}. The solvent gradient started at 40 % solvent B, rising to 43 % over 2 min, then stepped up to 50 %, and then 54 % over 10 min, after which the concentration was stepped up to 70 %. Finally, the percentage of B was raised to 99 % over 6 min before being returned to starting conditions of 40 % and left to re-equilibrate for 2 min.

Mass analysis was performed in MS^E-mode over an *m/z* range of 100–1200, in this mode the collision energy alternates every 100 ms between 6 V and a 20 V–30 V ramp. At lower energy, intact lipid ions are measured, whereas at elevated energy diagnostic fragment ions are generated to aid lipid identification. All data analyses were performed using SkyLine (v20.2) for relative quantification (Adams et al., 2020). Lipids were identified based on exact precursor mass, diagnostic fragment ions and chromatographic retention time.

To generate fatty acid methyl esters (FAMEs) for Gas Chromatography-Mass Spectrometry (GC–MS) analysis, concentrated lipid samples were resuspended in 1:1 (v/v) chloroform and trimethylsulfonium hydroxide (TMSOH) and subsequently analyzed using an Agilent 7890A GC system with a 30 m Agilent DB-FastFAME column (Agilent Technologies). Mass spectrometry was completed using a coupled Agilent 5975C MSD system (Agilent Technologies). FAME species were differentiated and determined by comparing to the FAME mix c4-24 standard (Sigma Aldrich). Data analysis was completed using the Agilent MassHunter Qualitative Navigator software (Agilent Technologies).

Lipooligosaccharide analysis

Overnight cultures of *A. baumannii* AB5075_UW were diluted to an OD_{600} of 0.05 in fresh LB media (20 ml) and grown to mid-log phase ($OD_{600} = 0.7$). A total of 1×10^9 cells were harvested by centrifugation 7,000 × *g* for 10 min, resuspended in 2 × lysis buffer and heated at 100℃ for 10 min. Samples containing cells were left to incubate with 0.5 $mg.mL^{-1}$ proteinase K (Sigma-Aldrich) at 56℃. Silver staining of *A. baumannii* LOS and lipid extracts was performed using an established method (Ascari et al., 2022). Densitometry analyses of lipid A bands were performed using Image Lab v6.1 software (Bio-Rad).

Lysozyme susceptibility analysis

The method to determine *A. baumannii* peptidoglycan integrity by probing time-dependent survival to lysozyme was adapted from a previously described protocol (Gil-Marqués et al., 2018). Overnight *A. baumannii* cells were resuspended in 10 mM HEPES (pH 7.5) and adjusted to $OD_{600} = 1.0$. A total of 128 μl cell suspension was added to 62 μL 10 mM EDTA, 10 μL Tris-HCl buffer (pH 8.0), with or without 1 $mg.mL^{-1}$ lysozyme in a 96-well plate. The rate of bacterial lysis was determined by measuring the OD_{600} at 2-minute intervals over 58 min (30 read cycles) at 25℃ with shaking in a SPECTROstar NANO Spectrophotometer (BMG Labtech). Cell absorbance data were normalized using GraphPad Prism 9.0. After 1 h, 50 μL of cell suspension from the plate were added to 950 μL of 1 × PBS and enumerated using an Attune™ NxT Acoustic Focusing Cytometer (Thermo Fisher). Bacterial cells were identified based on the forward scatter (FSC) and side scatter (SSC; Small Particle Filter) profiles, and comparison to PBS controls. A total of 10 μl from each sample was analyzed, of which cell death was defined by the difference in cell enumeration with or without lysozyme.

Results

Bioinformatic characterization of A. baumannii PgpA and PgpB

BLASTp searches identified PgpA (ABUW_0091) and PgpB (ABUW_0845) candidates in *A. baumannii* AB5075_UW. Although not identified in strain AB5075_UW, putative PgpC candidates were identified in some *A. baumannii* strains (16 %; The Acinetobacter-Dashboard). Hence, the absence of PgpC in *A. baumannii* AB5075_UW may be consistent with its reduced conservation across Gram-negative bacteria in general (Gasiorowski et al., 2019). To examine the fundamental features of the putative *A. baumannii* PgpA and PgpB candidates, we studied their structural models. Superimposition of the PgpA models from *A. baumannii* strain AB5075_UW and *E. coli* revealed a high degree of structural similarity (Fig. 1A & Figure S1). In contrast, *A. baumannii* PgpB lacked several alpha helices at both the periplasmic and cytoplasmic interface when compared to the *E. coli* counterpart (PDB: 5JWY, Fig. 1B) (Tong et al., 2016). However, we did identify the triangular phosphate binding site in *A. baumannii* PgpB (Fig. 1C), which consists of Lys-98, Arg-105 and Arg-165, and is in close proximity to residues His-124, His-171 and Asp-175 that constitute its catalytic triad (Tong et al., 2016). Hence, as anticipated, the core alpha-helical bundle containing the catalytic site of the enzyme is conserved between PgpB from the two distinct bacterial species. Initially, PgpA appeared core to the *Acinetobacter* genus as it was identified in 100 % of non-*A. baumannii* strains (179 genomes; The Acinetobacter-Dashboard) (Djahanschiri et al., 2022). Interestingly, some *A. baumannii* strains have lost this gene as the prevalence of PgpA across 292 *A. baumannii* genomes (extracted from PATRIC) was only 91 % across its 172 amino acids, only residues Val-83, Ile-84, Asn-85 and Leu-105 (based on PgpA from strain AB5075_UW) showed a sequence variation >10 % (Fig. 1A). PgpB was found to be highly conserved across the *Acinetobacter* genus, however, some strains of *Acinetobacter lwoffii* and *Acinetobacter brisouii* lacked the gene encoding this phosphatase, which included both clinical and environmental isolates (The Acinetobacter-Dashboard). Although previous studies have identified *pgpB* mutations in *A. baumannii* resistance evolution studies (Santos-Lopez et al., 2019, Zang et al., 2021a), this candidate was identified in > 98 % of *A. baumannii* strains and only a limited number of amino acid variations were seen across these 292 *A. baumannii* genomes (Fig. 1B).

To gain insight into the potentially diverse roles of PgpA and PgpB in *A. baumannii*, we examined the genetic loci of *pgpA* (A1S_3392/ABUW_0091) and *pgpB* (A1S_2734/ABUW_0845) in strains ATCC 17978 and AB5075_UW (Fig. 1D). These analyses revealed the co-localization of *pgpB* with the highly conserved RND efflux system *adeIJK*, a major antibiotic efflux system with implications in resistance to antimicrobial fatty acids (Damier-Piolle et al., 2008, Jiang et al., 2019). The genetic localization of *pgpA* in *A. baumannii* is similar to that of *E. coli*, with the flanking thiamine monophosphate kinase *thiL*, transcription antitermination factor *nusB* and riboflavin synthases *ribE* and *ribB1*.

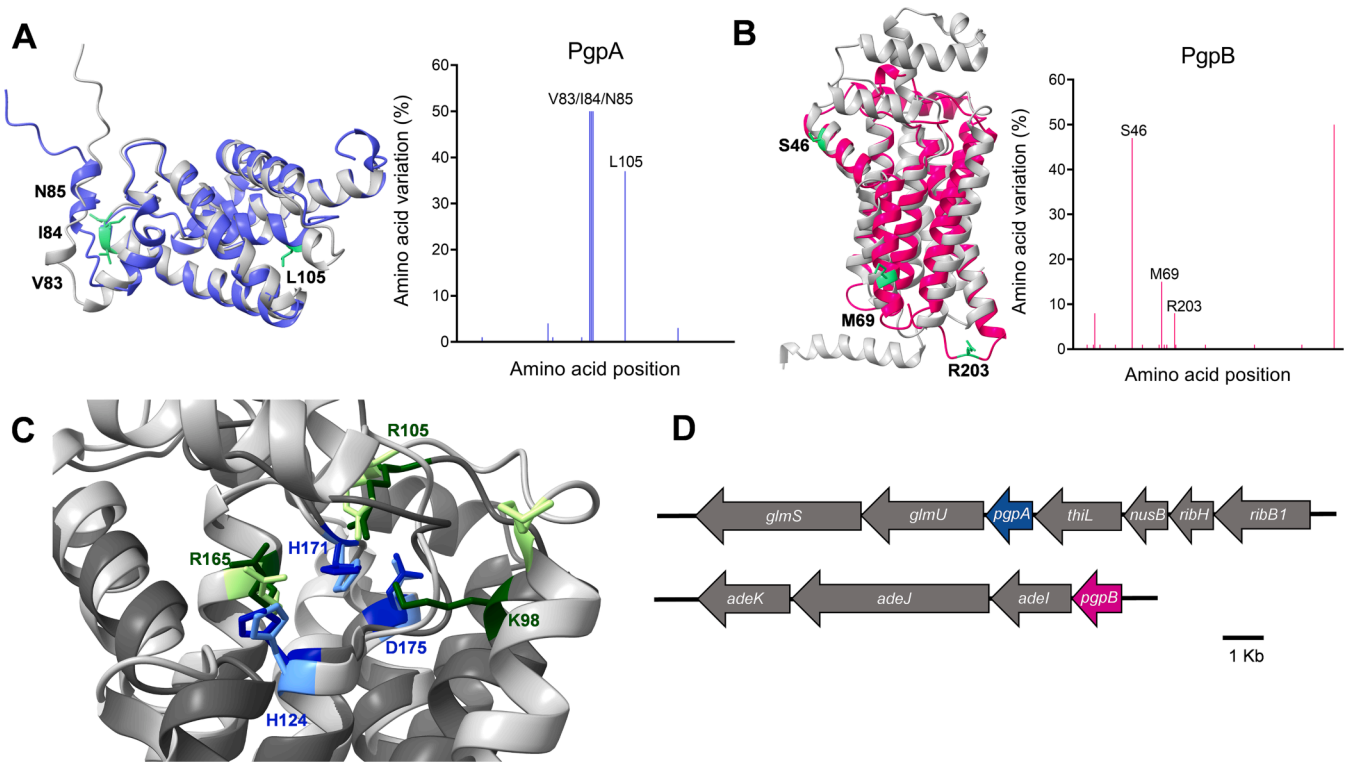

Fig. 1. Bioinformatic characterization of *A. baumannii* PgpA and PgpB. The AlphaFold 2.0 predicted structures of PgpA **(A,** blue**)** and PgpB **(B,** magenta**)** from *A. baumannii* AB5075_UW were superimposed onto the AlphaFold 2.0 model of *E. coli* PgpA and crystal structure of PgpB (5JWY), respectively (both in grey). Amino acid residues of PgpA (V83/I84/N85/L105) and PgpB (S46/M69/R203) with > 10 % amino acid variation across 292 *A. baumannii* strains were highlighted (green). **(C)** The PgpB structure of AB5075_UW (dark grey) was superimposed onto the structure of *E. coli* PgpB (light grey), from which residues responsible for phosphate binding in *E. coli* PgpB (light green) were identified in AB5075_UW PgpB (dark green). In addition, residues that belong to the catalytic triad that align across this binding site was also identified (*E. coli,* light blue; AB5075_UW, dark blue). All amino acid annotations refer to residues identified in *A. baumannii* PgpB. **(D)** The genetic clusters of *pgpA* and *pgpB* as seen in AB5075_UW, drawn to scale. (For interpretation of the references to color in this figure legend, the reader is referred to the web version of this article.)

Interestingly, *pgpA* is also co-localized with *glmS* and *glmU* in *A. baumannii*, which participate in the conversion of fructose-6-phosphate to UDP-GlcNAc, the precursor for the *de novo* synthesis of peptidoglycan (Barreteau et al., 2008). Overall, the genetic organization indicated that PgpA and PgpB may be linked to physiological processes in *A. baumannii* other than phospholipid biosynthesis.

PgpA plays a role in defining the lipid landscape of A. baumannii

To determine the impact of *pgpA* and *pgpB* on the relative abundance of the primary phospholipid species in *A. baumannii*, we performed Liquid Chromatography-Mass Spectrometry (LC-MS). Despite its proposed role in phosphatidylglycerol (PG) biosynthesis, our data revealed only minor changes within the major PG species in the *pgpA*::T26 and Δ*pgpA* mutants, as compared to their respective parental strains (Fig. 2A and B). The *A. baumannii* ATCC 17978 Δ*pgpB* mutant showed an increase in the abundance of PG(C16:0_C18:1), a phenotype not seen in strain AB5075_UW (Fig. 2B). Instead, the inactivation of *pgpA* resulted in dramatic shifts in various PE species, which was consistent in both *A. baumannii* isolates (Fig. 2A and B). Specifically, the mutation of *pgpA* significantly reduced the abundance of PE(C16:0_C18:1), but in turn, increased the abundance of PE(C16:1_C18:1) and PE(C18:1_C18:1). These changes in specific phospholipid species did not affect the total PE and PG pools (Figure S2A and B). Since acyl chain variations were observed by LC-MS, we next examined the distribution of the *A. baumannii* fatty acid species via Gas Chromatography-Mass Spectrometry (GC–MS). Consistently, inactivation of *pgpA*, but not *pgpB*, resulted in a significant increase in the desaturation status of the fatty acid pool with a ~ 2-fold increase in C16:1 and ~ 2-fold decrease in C16:0, in both *A. baumannii* backgrounds (Fig. 2C and D). Although considered a relatively low abundance species in *A. baumannii*, a significant decrease of C18:0 fatty acids was observed in the absence of either PgpA or PgpB (Figure S2C). These observations corroborate the LC-MS data, which also identified changes in phospholipids species with C16 acyl chains. We have previously reported on the role of DesA in desaturation of C16 fatty acids in *A. baumannii* (Adams et al., 2021a). However, we did not study whether this phospholipid desaturase acts upon C16 fatty acids associated with PE and/or PG species of phospholipids. Here we show that DesA is likely to be involved in the desaturation phenotype of the *pgpA* mutants, as DesA is primarily involved in synthesis of C16:1 in PE species, in both ATCC 17978 and AB5075_UW (Fig. 2E). Complementation of the *pgpA*::T26 mutant with wild-type *pgpA* reverted the 16:1 over-production to that observed for wild-type levels (Figure S3). Further, a Δ*pgpA*Δ*desA* double-mutant failed to adequately synthesize 16:1, similar to that observed in the Δ*desA* mutant (Figure S3). Collectively, these findings demonstrate that mutation of *A. baumannii* PgpA did not result in a quantifiable change in the abundance of PG, but rather the distribution of specific phospholipid species, possibly by virtue of enhanced DesA activity. The contribution of PgpB in *A. baumannii* phospholipid homeostasis was minimal.

We have previously identified that changes in the phospholipid composition, by exogenous fatty acid supplementation, impacts *A. baumannii* aminoglycoside resistance (Zang et al., 2021b). Hence, we assessed whether the altered membrane phospholipid makeup observed in this study also influenced aminoglycoside resistance. Indeed, mutation of *pgpA* resulted in a significant decrease in gentamicin and streptomycin resistance (Fig. 2F and G). The results were most striking in the multidrug resistant isolate AB5075_UW. Interestingly, the magnitude of

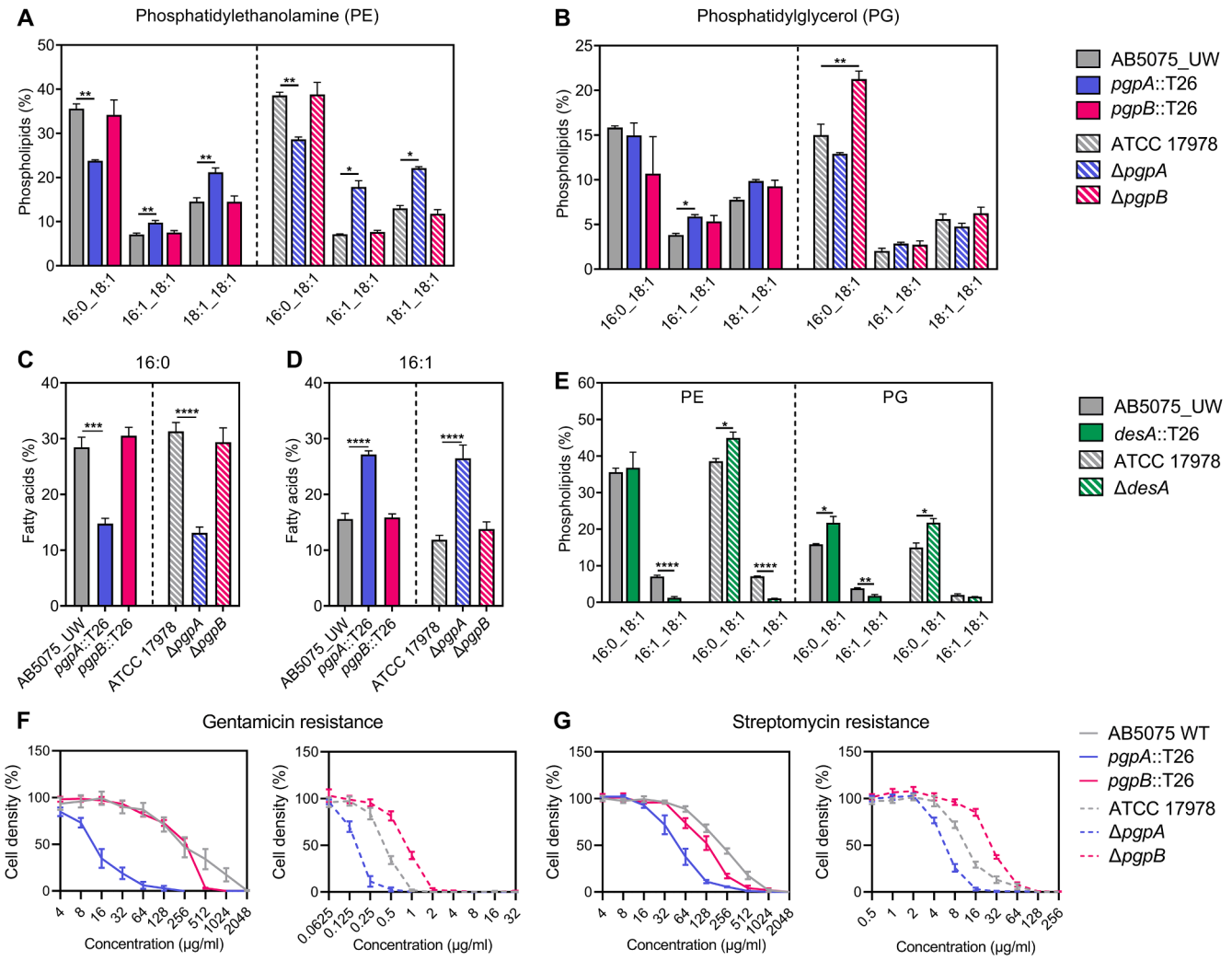

Fig. 2. The role of PgpA and PgpB in defining *A. baumannii*'s lipid landscape. The two major phospholipid species, phosphatidylethanolamine (PE) and phosphatidylglycerol (PG), were examined in AB5075_UW **(A)** and ATCC 17978 **(B)** strains using Liquid Chromatography-Mass Spectrometry (LC-MS), with species with an abundance > 1 % shown. Data represents the mean of at least biological triplicates (±SEM). The relative abundance of major *A. baumannii* fatty acid species: C16:0 **(C)**, C16:1 **(D)** in AB5075_UW and ATCC 17978 was determined by Gas Chromatography-Mass Spectrometry. Data represent the mean of at least biological quadruplicates (±SEM). The relative abundance of major PE and PG species **(E)** was examined in *desA*::T26 and Δ*desA* using LC-MS. Data represent the mean of at least biological triplicates (±SEM). Statistical analyses were performed using a one-way ANOVA (* = $p < 0.05$; ** = $p < 0.01$; *** = $p < 0.001$; **** = $p < 0.0001$). Resistance to gentamicin **(F)** and streptomycin **(G)** were determined in AB5075_UW and ATCC 17,978 wild-type, *pgpA* and *pgpB* mutants. Data were normalised against growth of cells without antibiotic supplementation and are representative of at least biological quadruplicates (±SEM).

change was comparable to that following the inactivation of a primary aminoglycoside efflux system, AdeAB (Figure S4C and E). As such, we also examined the resistance to pentamidine, which, like aminoglycosides, is effluxed by AdeAB. However, only small changes in pentamidine resistance were observed (Figure S4A and B). Further, AdeAB was not responsible for aminoglycoside efflux in strain ATCC 17978 (Figure S4D and F), which collectively indicate that PgpA-mediated aminoglycoside resistance is independent of AdeAB activity. Interestingly, the gentamicin susceptibility observed in the *pgpA* mutant is also unlikely to be exclusively due to C16:1 overaccumulation in the phospholipid pool, as the Δ*pgpA*Δ*desA* double mutant displayed increased susceptibility (Figure S3D). However, this may also be due to a loss of C16:1 beyond that observed for wild-type ATCC 17978 cells.

The impact of PgpA and PgpB across cell envelope biology

Considering the proposed alternative function of *pgpB* in *de novo* synthesis of peptidoglycan and the co-localization of *pgpA* with peptidoglycan biosynthesis genes, we assessed carbapenem susceptibility. A significant increase in susceptibility towards the peptidoglycan-targeting carbapenem antibiotics, imipenem and meropenem, was observed in the *pgpB*::T26 mutant (Fig. 3A and B). The lack of this phenotype in the ATCC 17978 Δ*pgpB* mutant may be a result of the inherent susceptibility of the strain towards this class of antibiotics. The impact of *pgpA* inactivation on carbapenem resistance was limited. As an alternative means of studying peptidoglycan integrity, lysozyme-mediated cell lysis was ascertained. Our data demonstrated a marked increase in the rate of cell death in *pgpB*::T26 compared to the wild-type, suggesting a weakened peptidoglycan in the absence of the inner membrane embedded phosphatase (Fig. 3C). We also noticed an impact of similar magnitude in *pgpA*::T26 in these analyses. Corroborating the carbapenem studies, the inactivation of *pgpA* and *pgpB* in ATCC 17978 did not significantly affect bacterial tolerance to lysozyme in this strain (Fig. 3D). Considering compromised peptidoglycan integrity can alter cell morphology (Vollmer et al., 2008), we examined the AB5075_UW strains via Differential Interference Contrast (DIC) microscopy. However, no significant impact was observed between the wild-type and the phosphatase mutants (Figure S5). Overall, these data indicate that PgpB

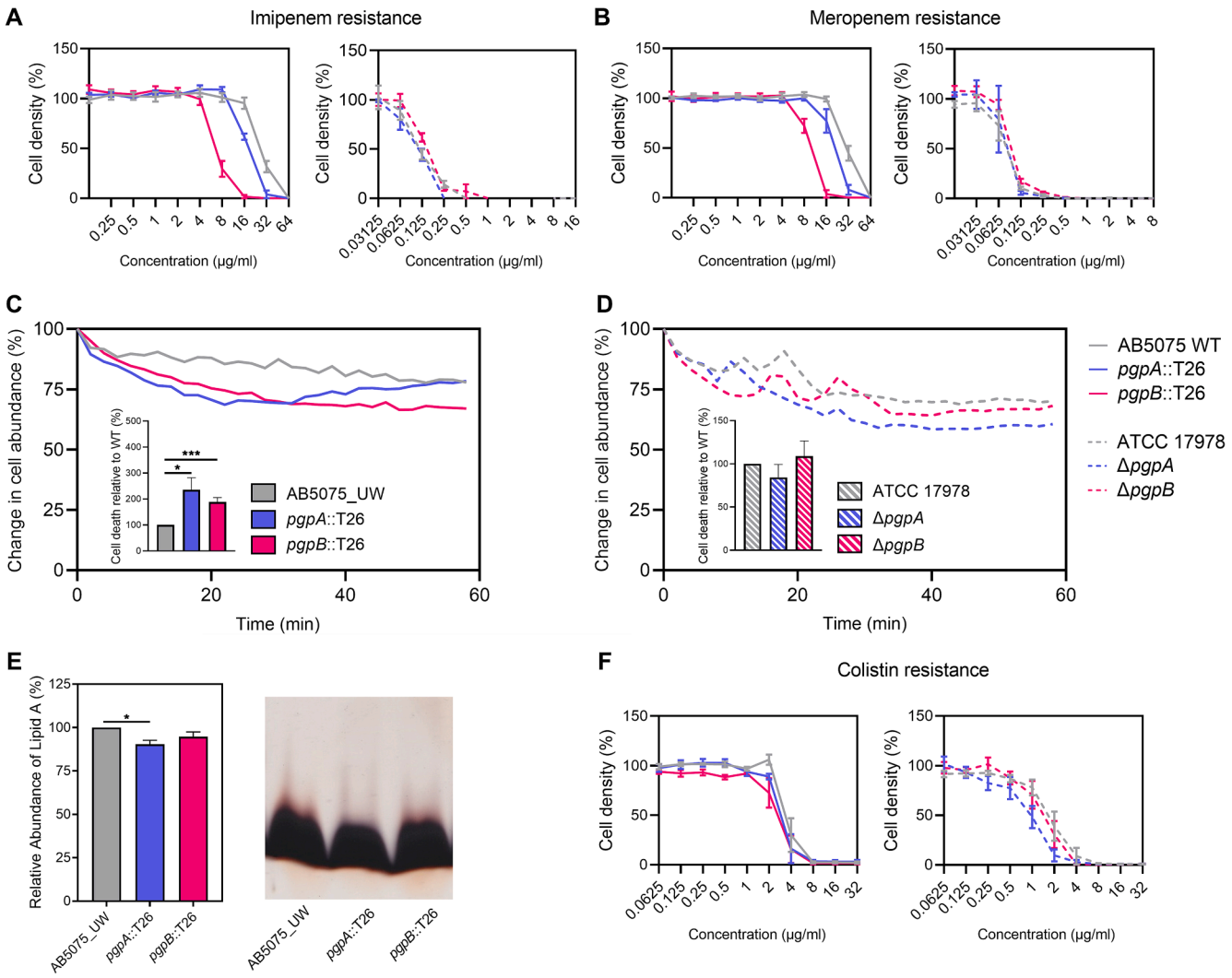

Fig. 3. The role of PgpA and PgpB in the biogenesis of *A. baumannii* peptidoglycan and lipid A. To determine the contribution of PgpA and PgpB in the maintenance of *A. baumannii* peptidoglycan, resistance to carbapenem antibiotics, imipenem **(A)** and meropenem **(B)** was determined. Data were normalized against growth of cells without antibiotic supplementation and are representative of at least biological quadruplicates (±SEM). Peptidoglycan integrity of AB5075_UW **(C)** and ATCC 17978 **(D)** was examined during lyzoyme and EDTA treatment for 60 min (OD_{600} readings, normalized). Cell death was enumerated via flow cytometry, and represents the difference in cell count with or without lysozyme. Data represent the mean of at least biological quadruplicates (±SEM). Statistical analyses were performed using a one-way ANOVA (* = $p < 0.05$; *** = $p < 0.001$). **(E)** Lipooligosaccharide of *A. baumannii* AB5075 wild-type, *pgpA*::T26 and *pgpB*::T26 were extracted from approximately 1×10^9 cells and visualized through SDS-PAGE and silver staining. Densitometry of lipid A was performed on biological quadruplicates from three independent experiments. Statistical analyses were performed using a one-way ANOVA (* = $p < 0.05$). Resistance to colistin **(F)** was examined, with data normalised against growth of cells without antibiotic supplementation. Data are representative of at least biological quadruplicates (±SEM).

contributes to peptidoglycan homeostasis, but this role may be ancillary as the protein does not appear to be critical for overall cell physiology.

We also quantitated *A. baumannii* lipid A via densitometry (Fig. 3E), as PgpB may harbor lipid A 1-phosphatase activity as previously characterized for LpxE in *E. coli* (Zhao et al., 2019). Further, dysregulation of phospholipids may impact upon the asymmetric outer member composition. Although no change was observed for *pgpB*::T26, the *pgpA*::T26 analysis revealed a minor role, which may be a pleiotropic effect of the dramatic remodeling of phospholipids in this mutant. Susceptibility to the lipid A-targeting antibiotic colistin was largely unaltered, with only a marginal increase in colistin susceptibility observed in the *A. baumannii* ATCC 17978 Δ*pgpA* mutant (Fig. 3F). Overall, these results suggest a limited correlation between the *A. baumannii* PGP phosphatases and this critical cell envelope component.

Discussion

The Gram-negative cell envelope in its defined multi-layered manner is the primary frontier against antibiotic assault. Understanding how biogenesis of core envelope layers, such as the phospholipids and peptidoglycan is coordinated by the bacterium is therefore of high importance. Although previously reported to mediate the biosynthesis of PG in *E. coli* (Lu et al., 2011), our phospholipid analysis indicated that the overall cellular abundance of PG in *A. baumannii* was not significantly altered upon the inactivation of *pgpA* or *pgpB*. However, it should be noted that the lack of impact on PG levels in the *A. baumannii* mutants does not suggest the absence of PGP phosphatase activity. The relative cellular abundance of PGP to PG is very low, indicating high total PGPase activity, possibly due to overlapping enzyme functionality or even redundancy in candidates such as PgpA and PgpB. Despite not being at quantifiable levels in our LC-MS analyses, PgpA inactivation may have led to a retardation in the PGP to PG conversion rate. *A. baumannii* harbors two distinct fatty acid desaturases, DesA and DesB (Adams et al., 2021a), of which only the former is capable of directly acting upon the acyl chains of phospholipids. Our new DesA findings have illustrated that this desaturase is directly responsible for introducing double bonds

in the C16 acyl chains of PE phospholipid species. Therefore, the lipidomic changes in the *pgpA* mutants, may be a result of DesA exerting greater desaturation activity, via as yet uncharacterized means.

PgpA was previously identified as a tobramycin-resistance determinant in both *A. baumannii* and *P. aeruginosa* (Gallagher et al., 2017, Gallagher et al., 2011). Here we demonstrated that resistance to other aminoglycosides, *e.g.* gentamicin and streptomycin, was drastically reduced following its inactivation. The magnitude of change was comparable to that following inactivation of a primary RND efflux system, AdeAB (Zang et al., 2021b). Considering the function of AdeAB is sensitive to changes in its local lipidomic composition, alteration of phospholipid distribution in *pgpA*::T26 may have perturbed its efflux capacity. However, resistance to pentamidine, also a substrate of AdeAB (Adams et al., 2018), was unaltered in *pgpA*::T26. In addition, although the dramatic reduction in aminoglycoside resistance was also observed in the ATCC 17978 Δ*pgpA* mutant, AdeAB is not responsible for aminoglycoside resistance in this strain. Instead, aminoglycoside antibiotics are known to gain entry to the bacterium primarily through membrane interactions (Serio et al., 2017). Hence, the PgpA-mediated phospholipid alterations may affect the overall biophysical properties of the membrane, thereby promoting uptake of this antibiotic.

The multifunctional nature of PAP2 enzymes highlights the extensive interconnectivity of cell envelope biogenesis pathways. During peptidoglycan synthesis, PgpB forms a functional complex with penicillin binding protein 1B (PBP1B), where peptidoglycan polymerization and C55-PP dephosphorylation are coupled, and loss of PgpB function may inhibit PBP1B to further promote C55-PP accumulation (Hernández-Rocamora et al., 2018). Hence, the increase in carbapenem susceptibility in *pgpB*::T26 observed in this study is likely due to the combination of impaired PBP1B activity and inhibition of PBPs by imipenem or meropenem. Considering the non-exclusivity of PgpB in C55-PP dephosphorylation, as *A. baumannii* is likely to harbor additional PAP2 candidates, *pgpB* inactivation may reduce, but not completely abolish, peptidoglycan polymerization and crosslinking in the periplasm. Indeed, our analyses revealed a significant increase in cell perturbation under lysozyme treatment in *pgpB*::T26, but the overall cell shape remained unaffected, which is a hallmark phenotype for mutants with severely compromised peptidoglycan structures. The lack of corresponding phenotypes in the ATCC 17978 strain may suggest strain-specific roles for these multifunctional phosphatases and/or distinct levels of functional redundancy with other members encoded by these respective strains. Indeed, the other putative PAP2 candidates were not always conserved across the species (data not shown) and therefore not included as candidates for mutagenesis to study the core contributors to *A. baumannii* envelope biogenesis.

A previous study reported on a colistin-resistant mutant of *A. baumannii* AB5075_UW which heavily supplements its LOS-deprived outer membrane with a near 2-fold increase in PG (Zhu et al., 2020). The authors suggested that both PgpA and PgpB played important roles in PG following the loss of LOS and colistin treatment, as cell growth was significantly attenuated in mutants of either phosphate. Our data indicated an unaltered resistance profile to colistin in LOS-replete *pgpA* or *pgpB* mutants of AB5075_UW or ATCC 17978. As such, the limited impact of the PGP phosphatases on the overall abundance of PG indicates a significant level of redundancy when the balance of other components of the envelope are appropriately maintained.

Taken together, our study has provided novel insights into the global roles of PGP-phosphatases (PgpA and PgpB) in membrane lipid homeostasis of the Gram-negative bacterium *A. baumannii*. This work has also illustrated the stringent coordination and striking interconnectivity of cell envelope biogenesis. The high level conservation of both PgpA and PgpB, and their overall implications in various aspects of antibiotic resistance underpin the importance of our core findings in microbial envelope biology.

Declaration of Competing Interest

The authors declare that they have no known competing financial interests or personal relationships that could have appeared to influence the work reported in this paper.

Acknowledgements

This work was supported by the National Health and Medical Research Council (Australia) through Project Grant 1159752 to B.A.E. M.Z. is a recipient of an Australian Government Research Training Program Scholarship.

Appendix A. Supplementary data

Supplementary data to this article can be found online at https://doi.org/10.1016/j.tcsw.2022.100092.

References

Adams, F.G., Stroeher, U.H., Hassan, K.A., Marri, S., Brown, M.H., 2018. Resistance to pentamidine is mediated by AdeAB, regulated by AdeRS, and influenced by growth conditions in *Acinetobacter baumannii* ATCC 17978. PLoS One 13. https://doi.org/10.1371/journal.pone.0197412.

Adams, K.J., Pratt, B., Bose, N., Dubois, L.G., St. John-Williams, L., Perrott, K.M., Ky, K., Kapahi, P., Sharma, V., Maccoss, M.J., Moseley, M.A., Colton, C.A., Maclean, B.X., Schilling, B., Thompson, J.W., 2020. Skyline for small molecules: a unifying software package for quantitative metabolomics. J. Proteome Res. 19, 1447–1458. https://doi.org/10.1021/acs.jproteome.9b00640.

Adams, F.G., Pokhrel, A., Brazel, E.B., Semenec, L., Li, L., Trappetti, C., Paton, J.C., Cain, A.K., Paulsen, I.T., Eijkelkamp, B.A., 2021a. *Acinetobacter baumannii* fatty acid desaturases facilitate survival in distinct environments. ACS Infectious Dis. 7, 2221–2228. https://doi.org/10.1021/acsinfecdis.1c00192.

Adams, F.G., Trappetti, C., Waters, J.K., Zang, M., Brazel, E.B., Paton, J.C., Snel, M.F., Eijkelkamp, B.A., 2021b. To make or take: bacterial lipid homeostasis during infection. mBio 12, e00928-21. https://doi.org/10.1128/mBio.00928-21.

Alquethamy, S., Ganio, K., Luo, Z., Hossain, S.I., Hayes, A.J., Ve, T., Davies, M.R., Deplazes, E., Kobe, B., Mcdevitt, C.A., 2022. Structural and biochemical characterization of *Acinetobacter baumannii* ZnuA. J. Inorg. Biochem. 231 https://doi.org/10.1016/j.jinorgbio.2022.111787.

Ascari, A., Tran, E.N.H., Eijkelkamp, B.A., Morona, R., 2022. Detection of a disulphide bond and conformational changes in *Shigella flexneri* Wzy, and the role of cysteine residues in polymerase activity. Biochim. Biophys. Acta Biomembr. 1864 https://doi.org/10.1016/j.bbamem.2022.183871.

Barák, I., Muchová, K., Wilkinson, A.J., O'toole, P.J., Pavlendová, N., 2008. Lipid spirals in *Bacillus subtilis* and their role in cell division. Mol. Microbiol. 68, 1315–1327. https://doi.org/10.1111/j.1365-2958.2008.06236.x.

Barreteau, H., Kovač, A., Boniface, A., Sova, M., Gobec, S., Blanot, D., 2008. Cytoplasmic steps of peptidoglycan biosynthesis. FEMS Microbiol. Rev. 32, 168–207. https://doi.org/10.1111/j.1574-6976.2008.00104.x.

Damier-Piolle, L., Magnet, S., Brémont, S., Lambert, T., Courvalin, P., 2008. AdeIJK, a resistance-nodulation-cell division pump effluxing multiple antibiotics in *Acinetobacter baumannii*. Antimicrob. Agents Chemother. 52, 557–562. https://doi.org/10.1128/AAC.00732-07.

Davies, M.R., Mcintyre, L., Mutreja, A., Lacey, J.A., Lees, J.A., Towers, R.J., Duchêne, S., Smeesters, P.R., Frost, H.R., Price, D.J., Holden, M.T.G., David, S., Giffard, P.M., Worthing, K.A., Seale, A.C., Berkley, J.A., Harris, S.R., Rivera-Hernandez, T., Berking, O., Cork, A.J., Torres, R.S.L.A., Lithgow, T., Strugnell, R.A., Bergmann, R., Nitsche-Schmitz, P., Chhatwal, G.S., Bentley, S.D., Fraser, J.D., Moreland, N.J., Carapetis, J.R., Steer, A.C., Parkhill, J., Saul, A., Williamson, D.A., Currie, B.J., Tong, S.Y.C., Dougan, G., Walker, M.J., 2019. Atlas of group A streptococcal vaccine candidates compiled using large-scale comparative genomics. Nat. Genet. 51, 1035–1043. https://doi.org/10.1038/s41588-019-0417-8.

Davis, J.J., Wattam, A.R., Aziz, R.K., Brettin, T., Butler, R., Butler, R.M., Chlenski, P., Conrad, N., Dickerman, A., Dietrich, E.M., Gabbard, J.L., Gerdes, S., Guard, A., Kenyon, R.W., Machi, D., Mao, C., Murphy-Olson, D., Nguyen, M., Nordberg, E.K., Olsen, G.J., Olson, R.D., Overbeek, J.C., Overbeek, R., Parrello, B., Pusch, G.D., Shukla, M., Thomas, C., Vanoeffelen, M., Vonstein, V., Warren, A.S., Xia, F., Xie, D., Yoo, H., Stevens, R., 2020. The PATRIC bioinformatics resource center: expanding data and analysis capabilities. Nucleic Acids Res. 48, D606–D612. https://doi.org/10.1093/nar/gkz943.

Djahanschiri, B., Di Venanzio, G., Distel, J.S., Breisch, J., Dieckmann, M.A., Goesmann, A., Averhoff, B., Göttig, S., Wilharm, G., Feldman, M.F., Ebersberger, I., 2022. Evolutionarily stable gene clusters shed light on the common grounds of pathogenicity in the *Acinetobacter calcoaceticus-baumannii* complex. PLoS Genet. 18 https://doi.org/10.1371/journal.pgen.1010020.

Edgar, R.C., 2004. MUSCLE: multiple sequence alignment with high accuracy and high throughput. Nucleic Acids Res. 32, 1792–1797. https://doi.org/10.1093/nar/gkh340.

Egan, A.J.F., Errington, J., Vollmer, W., 2020. Regulation of peptidoglycan synthesis and remodelling. Nat. Rev. Microbiol. 18, 446–460. https://doi.org/10.1038/s41579-020-0366-3.

Gallagher, L.A., Shendure, J., Manoil, C., 2011. Genome-scale identification of resistance functions in *Pseudomonas aeruginosa* using Tn-seq. mBio 2, e00315-10. https://doi.org/10.1128/mBio.00315-10.

Gallagher, L.A., Lee, S.A., Manoil, C., 2017. Importance of core genome functions for an extreme antibiotic resistance trait. mBio 8, e01655-17. https://doi.org/10.1128/mBio.01655-17.

Gasiorowski, E., Auger, R., Tian, X., Hicham, S., Ecobichon, C., Roure, S., Douglass, M.V., Trent, M.S., Mengin-Lecreulx, D., Touzé, T., Boneca, I.G., 2019. HupA, the main undecaprenyl pyrophosphate and phosphatidylglycerol phosphate phosphatase in *Helicobacter pylori* is essential for colonization of the stomach. PLoS Pathogens 15. https://doi.org/10.1371/journal.ppat.1007972.

Ghachi, M.E., Derbise, A., Bouhss, A., Mengin-Lecreulx, D., 2005. Identification of multiple genes encoding membrane proteins with undecaprenyl pyrophosphate phosphatase (UppP) activity in *Escherichia coli*. J. Biol. Chem. 280, 18689–18695. https://doi.org/10.1074/jbc.M412277200.

Gil-Marqués, M.L., Moreno-Martínez, P., Costas, C., Pachón, J., Blázquez, J., Mcconnell, M.J., 2018. Peptidoglycan recycling contributes to intrinsic resistance to fosfomycin in *Acinetobacter baumannii*. J. Antimicrob. Chemother. 73, 2960–2968. https://doi.org/10.1093/jac/dky289.

Hamidian, M., Nigro, S.J., 2019. Emergence, molecular mechanisms and global spread of carbapenem-resistant *Acinetobacter baumannii*. Microb. Genom. 5 https://doi.org/10.1099/mgen.0.000306.

Harding, C.M., Hennon, S.W., Feldman, M.F., 2017. Uncovering the mechanisms of *Acinetobacter baumannii* virulence. Nat. Rev. Microbiol. 16, 91. https://doi.org/10.1038/nrmicro.2017.148.

Hernández-Rocamora, V.M., Otten, C.F., Radkov, A., Simorre, J.-P., Breukink, E., Vannieuwenhze, M., Vollmer, W., 2018. Coupling of polymerase and carrier lipid phosphatase prevents product inhibition in peptidoglycan synthesis. Cell Surface 2, 1–13. https://doi.org/10.1016/j.tcsw.2018.04.002.

Icho, T., Raetz, C.R., 1983. Multiple genes for membrane-bound phosphatases in *Escherichia coli* and their action on phospholipid precursors. J. Bacteriol. 153, 722–730. https://doi.org/10.1128/jb.153.2.722-730.1983.

Jiang, J.H., Hassan, K.A., Begg, S.L., Rupasinghe, T.W.T., Naidu, V., Pederick, V.G., Khorvash, M., Whittall, J.J., Paton, J.C., Paulsen, I.T., Mcdevitt, C.A., Peleg, A.Y., Eijkelkamp, B.A., 2019. Identification of novel *Acinetobacter baumannii* host fatty acid stress adaptation strategies. MBio 10. https://doi.org/10.1128/mBio.02056-18.

Karakonstantis, S., Gikas, A., Astrinaki, E., Kritsotakis, E.I., 2020. Excess mortality due to pandrug-resistant *Acinetobacter baumannii* infections in hospitalized patients. J. Hospital Infect. 106, 447–453. https://doi.org/10.1016/j.jhin.2020.09.009.

Kearse, M., Moir, R., Wilson, A., Stones-Havas, S., Cheung, M., Sturrock, S., Buxton, S., Cooper, A., Markowitz, S., Duran, C., Thierer, T., Ashton, B., Meintjes, P., Drummond, A., 2012. Geneious Basic: an integrated and extendable desktop software platform for the organization and analysis of sequence data. Bioinformatics 28, 1647–1649. https://doi.org/10.1093/bioinformatics/bts199.

Koch, S., Exterkate, M., López, C. A., Patro, M., Marrink, S. J. & Driessen, A. J. M. 2019. Two distinct anionic phospholipid-dependent events involved in SecA-mediated protein translocation. Biochimica et Biophysica Acta (BBA) - Biomembranes, 1861, 183035. 10.1016/j.bbamem.2019.183035.

Lu, Y.H., Guan, Z., Zhao, J., Raetz, C.R., 2011. Three phosphatidylglycerol-phosphate phosphatases in the inner membrane of *Escherichia coli*. J. Biol. Chem. 286, 5506–5518. https://doi.org/10.1074/jbc.M110.199265.

Macdermott-Opeskin, H. I., Panizza, A., Eijkelkamp, B. A. & O'mara, M. L. 2022. Dynamics of the *Acinetobacter baumannii* inner membrane under exogenous polyunsaturated fatty acid stress. Biochimica et Biophysica Acta (BBA) - Biomembranes, 1864, 183908. 10.1016/j.bbamem.2022.183908.

May, K.L., Grabowicz, M., 2018. The bacterial outer membrane is an evolving antibiotic barrier. Proc. Natl. Acad. Sci. 115, 8852–8854. https://doi.org/10.1073/pnas.1812779115.

Mirdita, M., Schütze, K., Moriwaki, Y., Heo, L., Ovchinnikov, S., Steinegger, M., 2022. ColabFold - Making protein folding accessible to all. Nat. Methods 19, 679–682. https://doi.org/10.1038/s41592-022-01488-1.

Parsons, J.B., Rock, C.O., 2013. Bacterial lipids: metabolism and membrane homeostasis. Prog. Lipid Res. 52, 249–276. https://doi.org/10.1016/j.plipres.2013.02.002.

Pettersen, E.F., Goddard, T.D., Huang, C.C., Meng, E.C., Couch, G.S., Croll, T.I., Morris, J. H., Ferrin, T.E., 2021. UCSF ChimeraX: structure visualization for researchers, educators, and developers. Protein Sci 30, 70–82. https://doi.org/10.1002/pro.3943.

Santos-Lopez, A., Marshall, C.W., Scribner, M.R., Snyder, D.J., Cooper, V.S., 2019. Evolutionary pathways to antibiotic resistance are dependent upon environmental structure and bacterial lifestyle. eLife 8. https://doi.org/10.7554/eLife.47612.

Serio, A. W., Magalhães, M. L., Blanchard, J. S. & Connolly, L. E. 2017. Aminoglycosides: mechanisms of action and resistance. *In:* MAYERS, D. L., SOBEL, J. D., OUELLETTE, M., KAYE, K. S. & MARCHAIM, D. (eds.) *Antimicrobial Drug Resistance*. Cham: Springer International Publishing, pp. 213-229.

Sohlenkamp, C., Geiger, O., 2016. Bacterial membrane lipids: diversity in structures and pathways. FEMS Microbiol. Rev. 40, 133–159. https://doi.org/10.1093/femsre/fuv008.

Tian, X., Auger, R., Manat, G., Kerff, F., Mengin-Lecreulx, D., Touzé, T., 2020. Insight into the dual function of lipid phosphate phosphatase PgpB involved in two essential cell-envelope metabolic pathways in *Escherichia coli*. Sci. Rep. 10, 13209. https://doi.org/10.1038/s41598-020-70047-5.

Tickner, J., Hawas, S., Totsika, M., Kenyon, J.J., 2021. The Wzi outer membrane protein mediates assembly of a tight capsular polysaccharide layer on the *Acinetobacter baumannii* cell surface. Sci. Rep. 11, 21741. https://doi.org/10.1038/s41598-021-01206-5.

Tong, S., Lin, Y., Lu, S., Wang, M., Bogdanov, M., Zheng, L., 2016. Structural insight into substrate selection and catalysis of lipid phosphate phosphatase PgpB in the cell membrane. J. Biol. Chem. 291, 18342–18352. https://doi.org/10.1074/jbc.M116.737874.

Touzé, T., Tran, A.X., Hankins, J.V., Mengin-Lecreulx, D., Trent, M.S., 2008. Periplasmic phosphorylation of lipid A is linked to the synthesis of undecaprenyl phosphate. Mol. Microbiol. 67, 264–277. https://doi.org/10.1111/j.1365-2958.2007.06044.x.

Vollmer, W., Blanot, D., De Pedro, M.A., 2008. Peptidoglycan structure and architecture. FEMS Microbiol. Rev. 32, 149–167. https://doi.org/10.1111/j.1574-6976.2007.00094.x.

Wiegand, I., Hilpert, K., Hancock, R.E.W., 2008. Agar and broth dilution methods to determine the minimal inhibitory concentration (MIC) of antimicrobial substances. Nat. Protocols 3, 163–175. https://doi.org/10.1038/nprot.2007.521.

Zang, M., Adams, F.G., Hassan, K.A., Eijkelkamp, B.A., Kumar, A., Zgurskaya, H., 2021a. The impact of omega-3 fatty acids on the evolution of *Acinetobacter baumannii* drug resistance. Microbiol. Spectrum 9, e01455-21. https://doi.org/10.1128/Spectrum.01455-21.

Zang, M., Macdermott-Opeskin, H., Adams Felise, G., Naidu, V., Waters Jack, K., Carey Ashley, B., Ashenden, A., Mclean Kimberley, T., Brazel Erin, B., Jiang, J.-H., Panizza, A., Trappetti, C., Paton James, C., Peleg Anton, Y., Köper, I., Paulsen Ian, T., Hassan Karl, A., O'mara Megan, L., Eijkelkamp Bart, A., 2021b. The membrane composition defines the spatial organization and function of a major *Acinetobacter baumannii* drug efflux system. mBio 12, e01070-21. https://doi.org/10.1128/mBio.01070-21.

Zhao, J., An, J., Hwang, D., Wu, Q., Wang, S., Gillespie, A., Robert, Yang Eun, G., Guan, Z., Zhou, P., Chung Hak, S., Stephen Trent, M., Salama Nina, R., 2019. The lipid A 1-phosphatase, LpxE, functionally connects multiple layers of bacterial envelope biogenesis. mBio 10, e00886-19. https://doi.org/10.1128/mBio.00886-19.

Zhu, Y., Lu, J., Han, M.-L., Jiang, X., Azad, M., Patil, N.A., Lin, Y.-W., Zhao, J., Hu, Y., Yu, H.H., Chen, K., Boyce, J.D., Dunstan, R.A., Lithgow, T., Barlow, C.K., Li, W., Schneider-Futschik, E.K., Wang, J., Gong, B., Sommer, B., Creek, D.J., Fu, J., Wang, L., Schreiber, F., Velkov, T., Li, J., 2020. Polymyxins bind to the cell surface of unculturable *Acinetobacter baumannii* and cause unique dependent resistance. Adv. Sci. 7, 2000704. https://doi.org/10.1002/advs.202000704.